RSC Advances

PAPER

View Article Online
View Journal | View Issue

Cite this: *RSC Adv.*, 2021, **11**, 2783

Tungsten-substituted molybdophosphoric acid impregnated with kaolin: effective catalysts for the synthesis of 3,4-dihydropyrimidin-2(1*H*)-ones *via* biginelli reaction†

Dipak S. Aher,[a] Kiran R. Khillare,[a] Laxmikant D. Chavan[b] and Sunil G. Shankarwar*[a]

Received 19th November 2020
Accepted 4th January 2021

DOI: 10.1039/d0ra09811f

rsc.li/rsc-advances

A series of highly reusable heterogeneous catalysts (10–25 wt% PMo_7W_5/kaolin), consisting of tungsten-substituted molybdophosphoric acid, $H_3PMo_7W_5O_{40}\cdot 24H_2O$ (PMo_7W_5) impregnated with acid treated kaolin clay was synthesized by the wetness impregnation method. The newly synthesized catalyst was fully characterized using inductively coupled plasma-atomic emission spectroscopy (ICP-AES), Fourier transform infrared (FT-IR), powder X-ray diffraction (XRD), scanning electron microscopy (SEM), energy dispersive X-ray analysis (EDX), transmission electron microscopy (TEM), Brunauer–Emmett–Teller (BET) analysis and thermal analysis (TG-DTA). The synthesized materials were shown to be efficient in the synthesis of 3,4-dihydropyrimidin-2(1*H*)-ones *via* Biginelli reaction under solvent-free conditions. The obtained results indicate that 20% PMo_7W_5/kaolin catalyst showed remarkably enhanced catalytic activity compared to the bulk PMo_7W_5 catalyst, and also the (10 and 15%) PMo_7W_5 catalyst supported on kaolin clay.

1. Introduction

Heteropoly acids (HPA) are well known as environmentally benign and economically feasible alternatives to traditional acid catalysts due to their Brönsted acidity, high proton mobility and relatively better stability.[1–4] One of the important structural subclass of HPAs is the Keggin anion, which is typically represented by the general formula $XM_{12}O_{40}$,$^{x-8}$ where X is the central atom (Si, P, B, Zr *etc.*), x is its oxidation state, and M is the metal ion (Mo^{6+}or W^{6+}).[5–7] The M^{6+} ions can be replaced by many other metal ions, *e.g.*, V^{5+}, Co^{2+}, Zn^{2+}, Ni^{2+} *etc.*[8–12] The Keggin anion is composed of a central tetrahedral XO_4 surrounded by 12 edge and corner sharing metal-oxygen octahedra MO_6. The octahedra are arranged in four M_3O_{13} groups. Each group is formed by three octahedra sharing edges and having a mutual oxygen atom which is also shared with the central tetrahedral XO_4.[13,14] The catalytic properties of Keggin type heteropoly acids can be tuned by changing their central heteroatoms, framework poly-atoms, and charge-compensating cations because the substitution of these atoms changes their acid and redox properties.[15–17] It is well known that the acid strength of tungstophosphoric acid ($H_3PW_{12}O_{40}\cdot nH_2O$) is greater than that of molybdophosphoric acid ($H_3PMo_{12}O_{40}\cdot nH_2O$). Therefore, it can be projected that replacement of molybdenum (Mo) by tungsten (W) in the peripheral metal atom positions of the anions can increase the acid strength of the heteropoly acids, giving high catalytic activity for acid-catalyzed reactions.[18,19] Extremely low surface area, poor stability and rapid deactivation are the major problems associated with heteropoly acids.[20] Hence, it is imperative to employ an appropriate support to distribute the heteropoly acid.[21–25]

Kaolin, a clay mineral which is abundant on the earth, it is composed of abundantly 1 : 1 clay mineral $Al_2Si_2O_5(OH)_4$ structure per alumina-silicate producing bulky congested particles of SiO_4 tetrahedral sheets and $AlO_2(OH)_4$ octahedral sheets.[26,27] Kaolin clay are promising supports due to their common fascinating features, such as their inherent acidity, excellent thermal stability and easily controlled structural morphology.[28] Therefore, the acidified-kaolin with larger specific surface area is widely used as a very good catalyst carrier.[29] Actually, heteropoly acid-impregnated solid acids have caused great interests in many fields.[30,31]

3,4-Dihydropyrimidin-2-(1*H*)-ones (DHPM) are of significant interest in industry as well as in academia because of their promising biological and pharmacological activities such as antitumor, antibacterial, antiviral and anti-inflammatory activities.[32,33] DHPM also have some other interesting pharmacological properties of being calcium channel modulators, anti-HIV in some natural products containing the DHPM skeleton and anti-cancer by inhibiting kinesin motor protein.[34,35]

---

[a] *Department of Chemistry, Dr Babasaheb Ambedkar Marathwada University, Aurangabad, 431 004, M.S., India. E-mail: shankarwar_chem@yahoo.com*

[b] *Jawaharlal Nehru Engineering College, Aurangabad, 431003, M.S., India. E-mail: chavan@rediffmail.com*

† Electronic supplementary information (ESI) available. See DOI: 10.1039/d0ra09811f

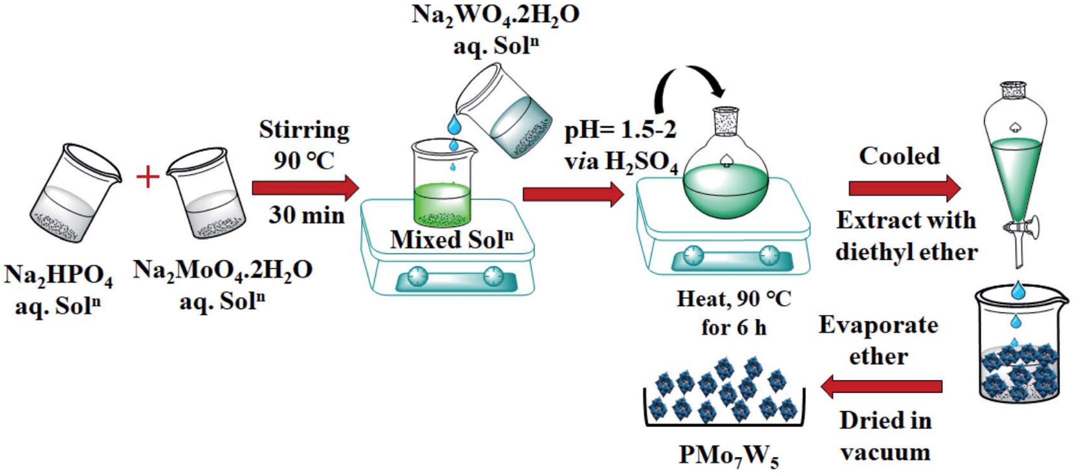

Scheme 1 Synthesis of tungsten-substituted molybdophosphoric acid, $H_3[PMo_7W_5O_{40}]\cdot 24H_2O$.

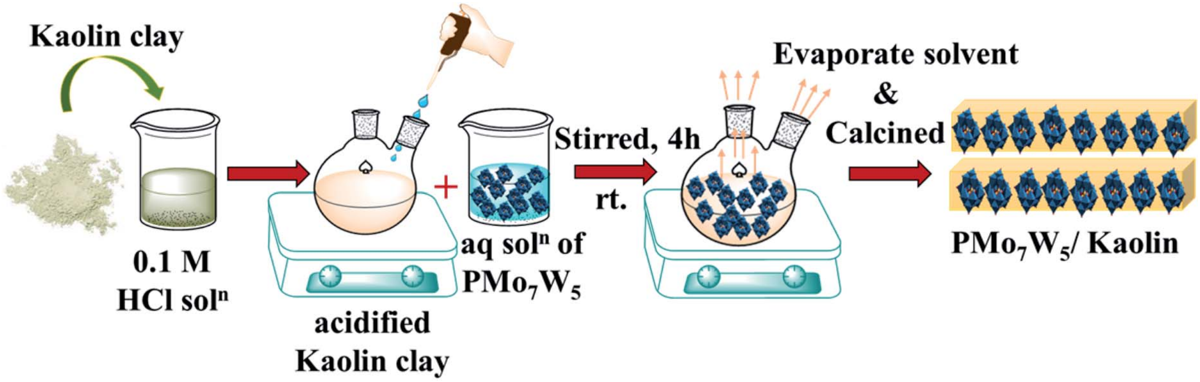

Scheme 2 Preparation of the series of catalysts having 10–25% loading of $H_3[PMo_7W_5O_{40}]\cdot 24H_2O$ on kaolin clay support.

Therefore, development of new, efficient and convenient protocols that lead to substituted DHPMs is of considerable attention. This has led to the recent disclosure of several one-pot methodologies for the synthesis of DHPM derivatives such as [bmim] [$FeCl_4$],[36] [bmim]BF_4-immobilized Cu(II) acetylacetonate,[37] piperidinium triflate[38] and ammonium carbonate.[39] However, some of existing methods associated with certain limitations such as environmental pollution caused by utilization of organic solvents, long reaction time, exotic reaction conditions and expensive catalysts. Therefore, it is crucial to further develop an efficient and convenient method to construct such significant scaffold (Scheme 1).

Encouraged by the intense ongoing research activity in the field of heterogeneous acid catalysis and in pursuit of our continuous interest in the area of catalysis by supported heteropoly acids.[40] Herein, we wish to report a simple, green and efficient protocol for the synthesis of 3,4-dihydropyrimidin-2(1*H*)-ones using series of tungsten-substituted molybdophosphoric acid ($H_3PMo_7W_5O_{40}\cdot 24H_2O$) impregnated with kaolin clay catalysts through Biginelli reaction (Scheme 2).

2. Experimental section

2.1 Materials and general characterization

Disodium phosphate (Na_2HPO_4), Sodium molybdate ($Na_2MoO_4\cdot 2H_2O$) sodium tungstate ($Na_2WO_4\cdot 2H_2O$) and kaolin clay (kaolin-product code: 15160) were purchased from MOLYCHEM in India and used without further purification. All the chemicals and solvents involved in the organic synthesis were purchased from Merck, Sigma Aldrich and Alfa Aesar.

Element content was measured on an ARCOS, Simultaneous ICP Spectrometer inductively coupled plasma atomic emission spectroscopy (ICP-AES). The Fourier-transform infrared spectroscopy (FTIR) spectrum was performed on a Bruker ALPHA (Eco-ATR) spectrophotometer. The materials were characterized by X-ray powder diffraction (XRD) using a Bruker AXS Company, D8 ADVANCE diffractometer (Germany). Scanning electron microscopy (SEM) images were obtained using a FEI Nova NanoSEM 450 combined with a Bruker XFlash 6I30 instrument for energy-dispersive X-ray spectroscopy (EDX), with a scanning electron electrode at 15 kV. Transmission electron microscopy (TEM) images were collected using a (HR-TEM: Jeol/JEM 2100) operated at an accelerating voltage of 200 kV. Nitrogen adsorption–desorption isotherms were measured with a NOVA Station A instrument at 77 K. The surface area calculated by the Brunauer–Emmett–Teller (BET) method and pore size distribution derived from adsorption branches of the isotherms using the distribution Barrett–Joyner–Halenda (BJH) method. The thermal stability of the sample was carried out using simultaneous thermogravimetry (TG) and differential thermal analysis (DTA) technique, measurements were performed using a SHIMADZU, DTG-60H simultaneous DTA-TG apparatus. The progress of the reaction monitored by thin-layer chromatography on Merck's silica plates and imagining accomplished by iodine/ultraviolet light. Melting points of all the synthesized analogues were resolute in open capillary tube and are uncorrected. ^{1}H and ^{13}C NMR spectra were recorded on a Bruker Avance 400 Spectrometer in DMSO and $CDCl_3$. Chemical shifts are expressed in δ parts per million relative to tetramethylsilane (TMS) as the internal standard. All yields refer to the isolated products.

2.2 Catalyst preparation

2.2.1 Preparation of $H_3[PMo_7W_5O_{40}]\cdot24H_2O$ (PMo_7W_5). HPA with general formula $H_3[PMo_7W_5O_{40}]\cdot24H_2O$, was synthesized using the procedure reported by Huixiong.[18] Briefly, Disodium phosphate (0.63 g, Na_2HPO_4) and desired amount of Sodium molybdate (7.48 g, $Na_2MoO_4\cdot2H_2O$) were dissolved in distilled water. The obtained solution was stirred at 90 °C. After being stirred for 30 min, aqueous solution of sodium tungstate (7.28 g, $Na_2WO_4\cdot2H_2O$) was added to the above heated solution. Subsequently, sulfuric acid (H_2SO_4) solution was added drop wise until the solution pH value reached about 1.5–2. The resulting mixture was heated at 90 °C for 6 h. Finally, the solution was cooled and extracted with diethyl ether in sulfuric acid environment. The powder $H_3[PMo_7W_5O_{40}]\cdot24H_2O$ was obtained after concentrated etherate solution was dried in vacuum.

2.2.2 Preparation of PMo_7W_5/kaolin. PMo_7W_5 impregnated-kaolin catalysts were prepared according to literature procedures with small modifications.[21] In a typical synthesis of 10% PMo_7W_5/kaolin, 0.5 g of PMo_7W_5 dissolved in 0.1 mol L^{-1} HCl solution was added into the flask containing 4.5 g of kaolin and stirred for 4 hours at room temperature. The resulting mixture was heated to 80 °C until complete evaporation of the liquid part. Then solid residue calcined in an oven at 200 K for 5 h. A series of PMo_7W_5/kaolin (10, 15, 20, 25 wt%) were prepared using the same method.

2.2.3 General procedure of the synthesis of 3,4-dihydropyrimidin-2(1*H*)-ones. In a typical experiment, a mixture of aromatic aldehyde (3 mmol), ethyl acetoacetate (3 mmol), urea (3.2 mmol) and 20% PMo_7W_5/kaolin (0.1 g) was stirred at 80 °C under solvent-free conditions for suitable time as indicated by thin-layer chromatography. After completion of reaction, the reaction mixture was diluted using hot ethanol (10.0 mL) and filtered for catalyst separation. The crude product was obtained by solvent evaporation under reduced pressure and recrystallized from ethanol. The recovered catalyst was washed with ethanol (10 mL) and dried overnight for further reuse. The physical data (Melting point, IR and H^1 & C^{13}NMR) of known compounds (see S5†) were found to be identical with those reported in the various literature.

3. Result and discussion

3.1 Catalyst characterization

3.1.1 ICP-AES analysis. The results of ICP-AES elemental analysis revealed that the atomic ratio of P/Mo/W is nearly maintained 1.05 : 6.68 : 5.18 which corresponds to the formula $H_3[PMo_7W_5O_{40}]\cdot24H_2O$ (PMo_7W_5).[18,40]

3.1.2 FT-IR spectroscopy. Primarily, FT-IR spectroscopy was used to confirm the successful functionalization of the PMo_7W_5/kaolin catalyst (Fig. 1). For bulk PMo_7W_5, characteristic bands exhibiting at 1061 (P–O_a in central tetrahedral), 960 (terminal M=O_d), 873 (M–O_b–M), and 757 cm^{-1} (M–O_c–M) are accorded with asymmetric vibrations in Keggin unit.[17] In the FT-IR spectrum of kaolin, absorptions at 748 cm^{-1} and 789 cm^{-1} are attributed to Si–O–Al vibrations and the band at 915 cm^{-1} is assigned to Al-OH bending vibrations. The peak at 1007 cm^{-1} is assigned to Si–O–Si in-plane vibrations and at 1113 cm^{-1} is assigned to asymmetric Si–O–Si stretching vibrations.[26] The spectrum of PMo_7W_5/kaolin with different percentages of PMo_7W_5 showed two bands at 938 and 910 cm^{-1}, which might be attributed to the (terminal M=O_d) and (M–O_b–M), respectively. However, the bands at 1061 and 757 cm^{-1} were not prominent due to overlapping with the strong bands of silica in the kaolin support.[21]

3.1.3 XRD analysis. Fine dispersion of PMo_7W_5 on the kaolin support was confirmed by XRD analysis. Fig. 2 shows the

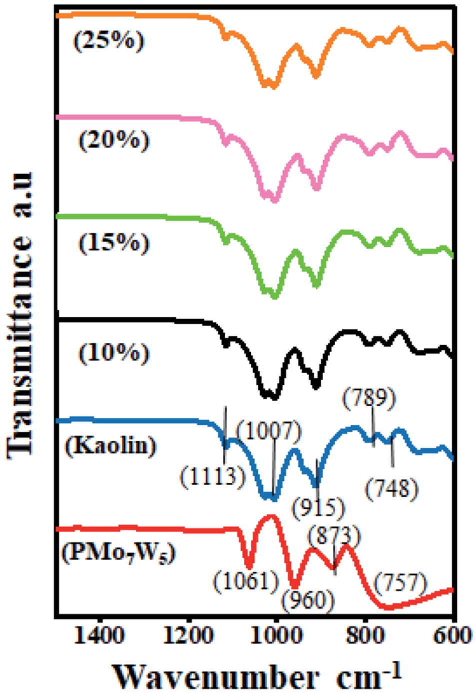

Fig. 1 FT-IR analysis of bulk PMo_7W_5, kaolin and PMo_7W_5/kaolin composites.

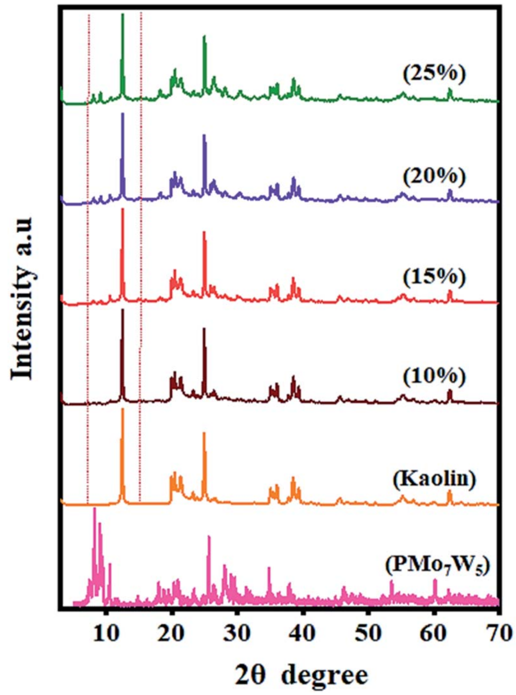

Fig. 2 XRD patterns of bulk PMo_7W_5, kaolin and PMo_7W_5/kaolin composites.

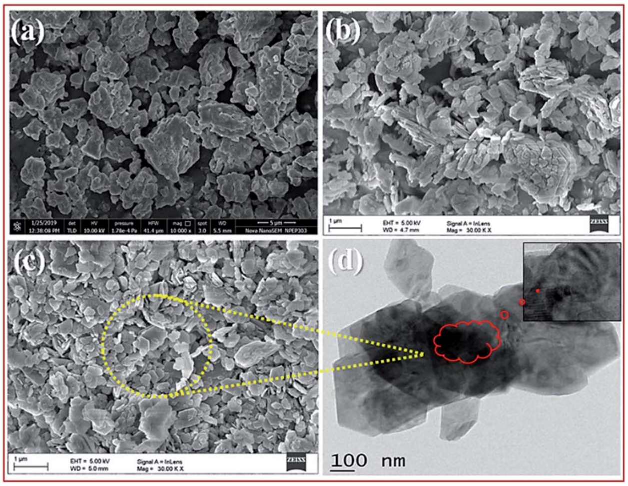

Fig. 3 FE-SEM images of bulk PMo_7W_5 (a), kaolin (b), 20% PMo_7W_5/kaolin (c) and TEM images of 20% PMo_7W_5/kaolin (d).

XRD patterns of PMo_7W_5, kaolin support and PMo_7W_5/kaolin composites (with PMo_7W_5 loading from 10, 15, 20 and 25%). Unsupported PMo_7W_5 showed the characteristic XRD peaks of the Keggin structure mainly exist in four ranges of $2\theta = 7–10°$, 18–23°, 25–30° and 31–37° (ref. [17]) On the other hand, several prominent peaks of kaolin detected at about $2\theta = 12.36°$, 20.44°, 21.42°, 25.10°, 35.03°, 38.48° and 62.38°. The peak at $2\theta = 12.36°$ is the distinctive XRD form of kaolin.[41] Interestingly, 10, 15, 20 and 25% PMo_7W_5/kaolin catalyst exhibited no characteristic peaks of PMo_7W_5 but showed almost the same XRD pattern as kaolin, indicating the retention of the original characteristics of kaolin clay.[42] The above results strongly supports that PMo_7W_5 was finely and molecularly dispersed on the kaolin support in the PMo_7W_5/kaolin catalyst.[28,43]

Table 1 Textural properties of the prepared catalyst

Entry	Samples	S_{BET} ($m^2 g^{-1}$)	D_{pore} (nm)	V_{pore} ($cm^3 g^{-1}$)
1	PMo_7W_5	5.3801	10.409	0.014
2	Kaolin clay	16.093	15.850	0.070
3	20% PMo_7W_5/kaolin	6.199	3.882	0.036

3.1.4 SEM and TEM analysis. The surface morphology and texture of produced samples was investigated using SEM and TEM analysis (Fig. 3a–d). As seen in Fig. 3a, the irregularly shaped particles with rough, flaky edges were observed for bulk PMo_7W_5 sample. The SEM images of kaolin and 20% PMo_7W_5/kaolin are shown in Fig. 3b and c respectively. These images clearly show that the surface morphology of supported catalyst is almost identical to that of pure kaolin. No change in surface morphology of the catalyst demonstrate that PMo_7W_5 species are well dispersed inside the hexagonal pores.[41] Further, no separate crystallites of bulk phase of PMo_7W_5 were found in 20% PMo_7W_5/Kaolin.

The TEM images of 20% PMo_7W_5/kaolin (Fig. 3d) shows that most of the hexagonal pores covered with dark colored fine particles. This indicates uniform dispersion of PMo_7W_5 inside the hexagonal pores of kaolin clay support.

3.1.5 EDX analysis and mapping images. The chemical constitution of bulk PMo_7W_5 and 20% PMo_7W_5/kaolin were evidenced by EDX analysis as depicted in Fig. S2.† The results of newly prepared PMo_7W_5 confirms the presence of P, Mo and W (Fig. S1-a†). Moreover, the EDX results of 20% PMo_7W_5/kaolin (Fig. S2-b†) showed the presence of P, Mo and W elements of PMo_7 W_5 and Si, Al and O of kaolin clay. Which strongly indicates the successfully formation of 20% PMo_7W_5/kaolin.[42]

Additionally, EDS mapping images proved a uniform distribution of W, Mo and P in the desired PMo_7W_5 catalyst system (Fig. 4a). The elemental mapping of Fig. 4b depicted the construction of a well-dispersed composite material of P, Mo, W, Si, Al and O in the synthesized 20% PMo_7W_5/kaolin catalyst, which is in moral contract with FT-IR, XRD and SEM results.

3.1.6 BET analysis. The specific surface area is an important representative of a catalyst. The specific surface area, pore diameter, and pore volume of the catalysts were determined by BET and BJH methods. The specific surface area of the PMo_7W_5, kaolin support and 20% PMo_7W_5/kaolin catalysts were 5.3801, 16.093 and 6.199 $m^2 g^{-1}$, respectively (Table 1). The porosities of these catalysts was investigated by N_2 adsorption/desorption measurement. N_2 adsorption/desorption isotherm are the type IV in nature according to the IUPAC classification. The bulk PMo_7W_5 exhibit a well expressed H4 hysteresis loop (Fig. 5a), whereas, parent kaolin clay and 20% PMo_7W_5/kaolin catalyst exhibit H3 hysteresis loop (Fig. 5b and c) in the range of 0.4–1.0 P/P_0 at high relative pressure, which is typical for mesoporous

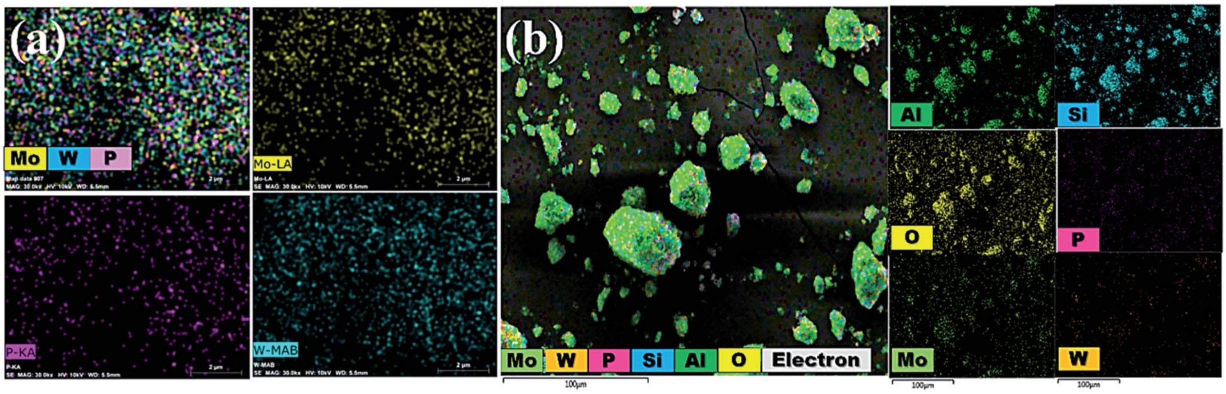

Fig. 4 Elemental mapping images of (a) bulk PMo_7W_5 (b) 20% PMo_7W_5/kaolin catalyst.

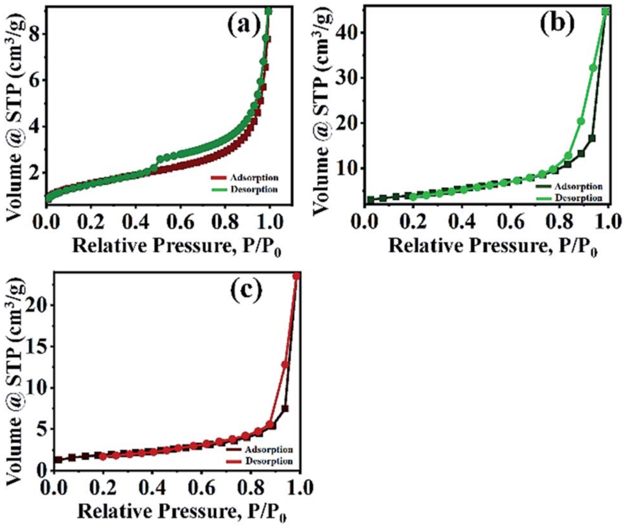

Fig. 5 N_2 adsorption–desorption isotherms of (a) PMo_7W_5 (b) kaolin support (c) 20% PMo_7W_5/kaolin.

materials. As demonstrated in Table 1, the pore diameter of the PMo_7W_5, kaolin support and 20% PMo_7W_5/kaolin catalyst were 10.409, 15.850, and 3.882 nm respectively. Also pore volume (0.014–0.070 cm^3 g^{-1}) of the catalysts were calculated using the BJH method (see Fig. S3-a–c†).[26,44,45]

The study proven that the surface area of 20% PMo_7W_5/kaolin catalyst slightly increased but not more than that of kaolin support.[46] This could primarily due to deposition and incorporation of PMo_7W_5 catalyst into the pores of kaolin support.[47]

3.1.7 TG-DT analysis. The thermal stability of bulk PMo_7W_5 and 20% PMo_7W_5/kaolin examined by the thermogravimetric (TG) and differential thermal analysis (DTA). The hydrated solids usually obtained with a large amount of water of crystallization. Generally, three types of crystallographic water molecule could be distinguishes in the hydrated solid (Fig. 6a).[48,49] The TG curve for bulk PMo_7W_5 shows the total weight loss of 16.01% below 460 °C indicating that 24 water molecules calculated were lost. The first mass loss stage, free

Scheme 3 Synthesis of ethyl 6-methyl-2-oxo-4-aryl-1,2,3,4-tetrahydropyrimidine-5-carboxylate (**4a–n**) by using 20% PMo_7W_5/kaolin catalyst.

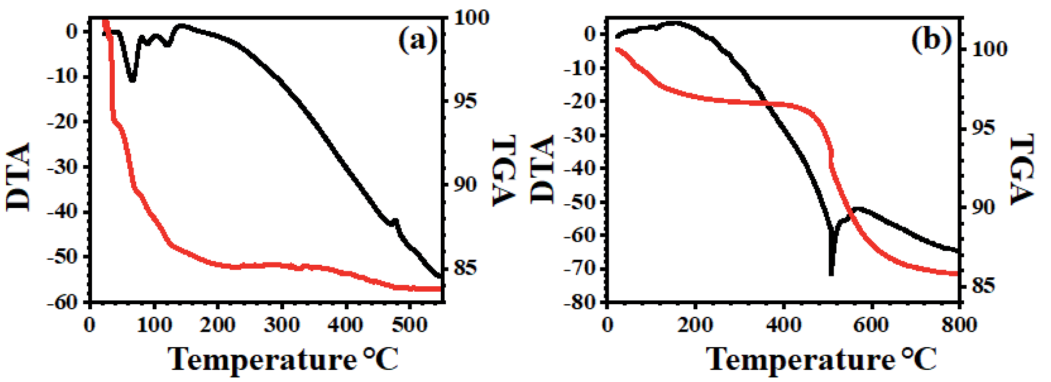

Fig. 6 TG-DT analysis of (a) PMo_7W_5 and (b) 20% PMo_7W_5/kaolin catalyst.

Table 2 Effect of $H_3PMo_7W_5O_{40}\cdot 24H_2O$ loading on support kaolin for the synthesis of ethyl 6-methyl-2-oxo-4-phenyl-1,2,3,4-tetrahydropyrimidine-5-carboxylate (**4a**)[a]

Entry	Catalyst	Time[b] (min)	Yield[c] (%)
1	Pure kaolin	120	45
2	Bulk $H_3PMo_7W_5O_{40}\cdot 24H_2O$	55	60
3	10% PMo_7W_5/kaolin	35	68
4	15% PMo_7W_5/kaolin	20	85
5	20% PMo_7W_5/kaolin	08	95
6	25% PMo_7W_5/kaolin	08	95

[a] Reaction conditions: benzaldehyde (3 mmol), ethyl acetoacetate (3 mmol), urea (3.2 mmol) and PMo_7W_5/kaolin catalyst. [b] Reaction progress monitored by TLC. [c] Isolated yields.

Table 3 Effect of temperature and amount of catalyst on ethyl 6-methyl-2-oxo-4-phenyl-1,2,3,4-tetrahydropyrimidine-5-carboxylate (**4a**)[a]

Entry	Catalyst (mg)	Temp. °C	Time[b]	Yield[c] (%)
1	0	80	24 h	Trace
2	25	80	8 min	65
3	50	80	8 min	70
4	70	80	8 min	82
5	100	80	8 min	95
6	125	80	8 min	95
7	100	70	8 min	65
8	100	60	8 min	45

[a] Reaction conditions: benzaldehyde (3 mmol), ethyl acetoacetate (3 mmol), urea (3.2 mmol) and 20% PMo_7W_5/kaolin catalyst. [b] Reaction progress monitored by TLC. [c] Isolated yields.

crystalized water, 10.20% of the total sample mass was lost and an endothermic peak appeared at 95 °C for 15-water molecule. The second mass lost for H^+ -combined water, about 3.27% of the total sample mass was loss and endothermic peak appeared at 147 °C for 4.9 water molecule. The structure water, 2.5% of the total sample mass loss and DTA curve shows the exothermic peak at 467 °C, which demonstrate stability of Keggin unit and these third mass losses for oxide mixture.

The TG-DTA of supported PMo_7W_5 on kaolin showed the mass loss of about 3.51% up to 430 °C temperature corresponds to dehydration of surface and interlayer water molecules (Fig. 6b). The gradual mass loss about 7.19% within the temperature range 430 °C to 750 °C, which indicates an increase in the thermal stability of bulk PMo_7W_5 on kaolin clay support.[40] This might be due to formation of intermolecular bonding interaction between kaolin and bulk PMo_7W_5. The above result reveals that strong chemical interaction between kaolin and PMo_7W_5 catalyst.

3.2 Catalytic activity

Table 4 Effect of different solvents on the ethyl 6-methyl-2-oxo-4-phenyl-1,2,3,4-tetrahydropyrimidine-5-carboxylate (**4a**)[a]

Entry	Catalyst (mg)	Temp. °C	Solvent	Time[b]	Yield[c] (%)
1	100	Reflux	EtOH	15 min	72
2	100	Reflux	H_2O	10 min	68
3	100	Reflux	MeOH	25 min	62
4	100	Reflux	CH_3CN	45 min	45
5	100	80	DMF	65 min	55
6	100	Reflux	CH_2Cl_2	30 min	59
7	100	80	Solvent-free	8 min	95

[a] Reaction conditions: benzaldehyde (3 mmol), ethyl acetoacetate (3 mmol), urea (3.2 mmol) and 20% PMo_7W_5/kaolin catalyst. [b] Reaction progress monitored by TLC. [c] Isolated yields.

Our initial studies were focused on the optimization of the reaction conditions for the synthesis of ethyl 6-methyl-2-oxo-4-aryl-1,2,3,4-tetrahydropyrimidine-5-carboxylate derivatives. Benzaldehyde (3 mmol), ethyl acetoacetate (3 mmol) and urea (3.2 mmol) were chosen as substrates for model reaction (Scheme 3).

Table 5 Synthesis of ethyl 6-methyl-2-oxo-4-aryl-1,2,3,4-tetrahydropyrimidine-5-carboxylate (**4a–n**) by using 20% PMo_7W_5/kaolin catalyst[a,b]

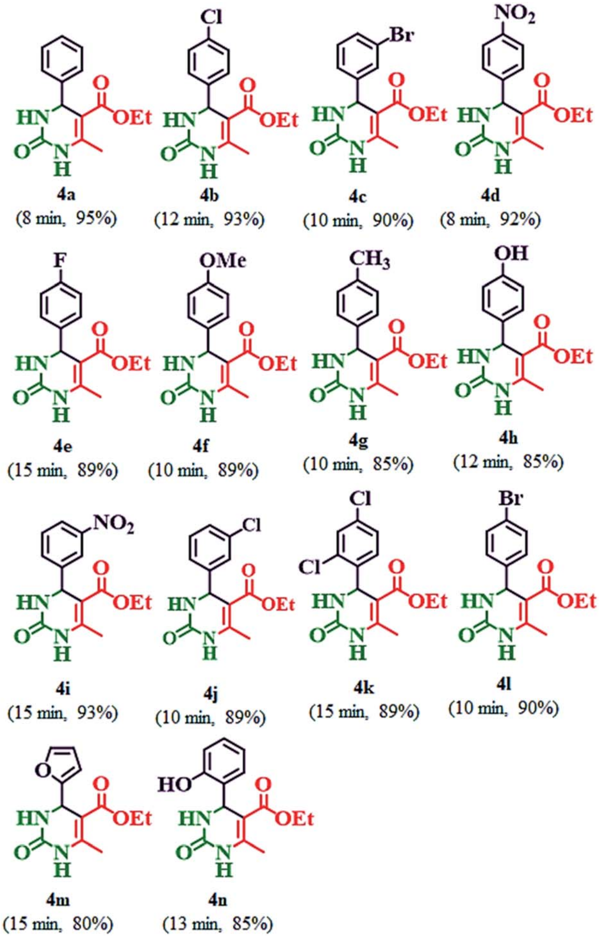

[a] Reaction conditions: aldehydes (**4a–n**) (3 mmol), ethyl acetoacetate (3 mmol), and urea (3.2 mmol) in 20% PMo_7W_5/kaolin (0.1 g) stirred at 80 °C. [b] Isolated yields.

Table 6 Biginelli reaction of benzaldehyde, ethyl acetoacetate and urea with different catalysts[a]

Entry	Catalyst	Condition	Time	Yield[b] (%) Ref
1	*p*-Sulfonic acid calixarenes	EtOH, reflux	8 h	69 (ref. [50])
2	$NH_4H_2PO_4$/MCM-41	Solvent-free, 100 °C	6 h	72 (ref. [51])
3	$[Et_3NH]$ $[HSO_4]$	Solvent-free, 100 °C	1 h	75 (ref. [52])
4	12-Tungstophosphoric acid	Reflux, acetic acid	6 h	98 (ref. [53])
5	[Btto][*p*-TSA]	Solvent-free, 90 °C	30 min	96 (ref. [54])
6	Fe_3O_4/PAA-SO_3H	Solvent-free, rt	2 h	90 (ref. [55])
7	$SnCl_2$/nano SiO_2	EtOH, reflux	40 min	94 (ref. [56])
8	Bentonite/PS-SO_3H	Solvent-free, 120 °C	30 min	89 (ref. [57])
9	Fe_3O_4@SBA-15	EtOH, 90 °C	6 h	85 (ref. [58])
10	PS-PEG-SO_3H	Dioxane & 2-propanol, 80 °C	10 h	80 (ref. [59])
11	20% PMo_7W_5/kaolin	Solvent-free, 80 °C	8 min	95 (this work)

[a] Reaction conditions: benzaldehydes (3 mmol), ethyl acetoacetate (3 mmol), and urea (3.2 mmol) in 20% PMo_7W_5/kaolin (0.1 g) stirred at 80 °C. [b] Isolated yields.

Table 7 Recycling and reuse of the catalyst[a]

Entry	Number of recycle	Yield (%)[b]
1	1	95
2	2	95
3	3	94
4	4	90
5	5	90
6	6	88

[a] Reaction conditions: benzaldehyde (3 mmol), ethyl acetoacetate (3 mmol), urea (3.2 mmol) and 20% PMo_7W_5/kaolin catalyst, time 8 min. [b] Isolated yields.

Various amounts of PMo_7W_5/kaolin were used to study the effect of the composition of the catalyst on the conversion and obtained results are summarized in Table 2. Pure kaolin showed extremely low catalytic activity in terms of the reaction time and the yield of the desired product (Table 2, entry 1). Bulk PMo_7W_5 gave a moderate yield of the product but only after an extended reaction time (Table 2, entry 2). It was observed that both yield of the product and reaction time were improved upon increasing the catalyst loading up to 20% w/w (Table 2, entries 3, 4, and 5). Further, an increase in PMo_7W_5 catalyst loading above 20% w/w on kaolin support have no effect on yield of product and reaction time due to leaching of catalyst from the support (Table 2, entry 6). The increase in activity of the 20% PMo_7W_5/kaolin catalyst was due to high dispersion of PMo_7W_5 catalyst on kaolin support. This would lead to an increase in its surface area and the number of active sites compared with the bulk PMo_7W_5 catalyst. Hence, 20% PMo_7W_5/kaolin catalyst was found to be optimal amount and adequate to push the reaction forward.

The determination of appropriate amount of the catalyst for catalyzing the reaction is another critical parameter in terms of reaction efficiency. To find appropriate amount of catalyst, the model reaction was carried out in the presence of different amounts (25, 50, 70, 100 and 125 mg) of 20% PMo_7W_5/kaolin and obtained results are summarized in Table 3. When the amount of 20% PMo_7W_5/kaolin increases gradually, product yield also increases (Table 3, entries 1–5). The obtained results demonstrates that 100 mg amount of 20% PMo_7W_5/kaolin catalyst gave 95% yield of product at 80 °C (Table 3, entry 5). Additional increase in the amount (125 mg) of 20% PMo_7W_5/kaolin does not increase in the yield of the product (Table 3, entry 5). This may be due to overtiredness of the catalytic site or

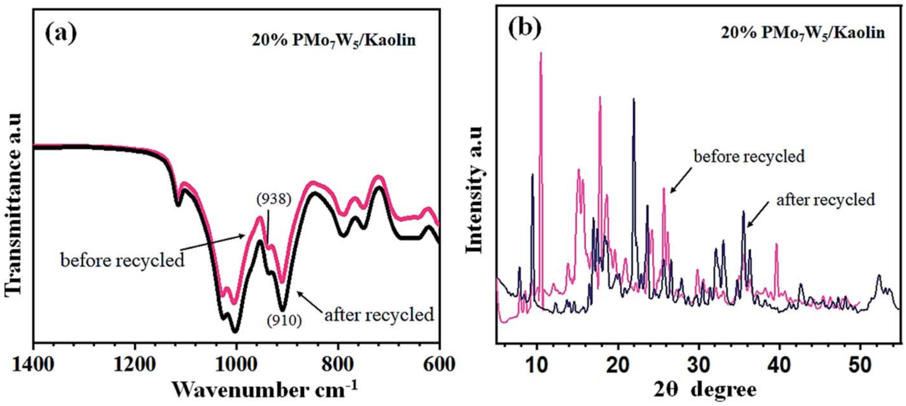

Fig. 7 FT-IR (a) and XRD (b) analysis of recovered 20% PMo_7W_5/kaolin catalyst.

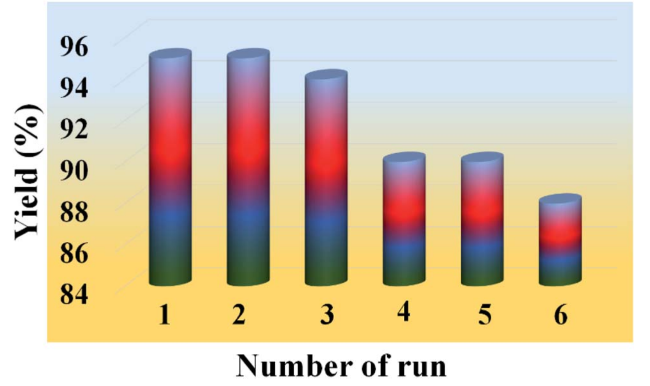

Fig. 8 Recyclability test of 20% PMo_7W_5/kaolin catalyst on model reaction.

accomplishment of the maximum conversion efficiency of the catalyst. It is also important to note that at 60 and 70 °C low to moderate conversion observed, whereas at 80 °C excellent conversion of starting material were seen (Table 3, entry 5 *versus* entries 7 and 8). The effectiveness of model reaction also studied without using any catalyst. Where, trace amount of the product obtained after a long period (Table 3, entry 1).

Further, the efficiency of 20% PMo_7W_5/kaolin was investigated by using 100 mg of 20% PMo_7W_5/kaolin in various organic solvents (Table 4). Initially, the model reaction was carried out in ethanol and water at reflux temperature the moderate yield were obtained (Table 4, entries 1, 2). When the methanol, acetonitrile, dichloromethane were used as solvent at reflux temperature and DMF at 80 °C, it gave lower yields of product (Table 4, entries 3–6). None of the above solvents demonstrates the advantage of time and yield instead of solvent-free condition (Table 4, entry 7). Therefore, solvent-free condition was superior in terms of cost and it is environmentally benign to promote further derivatives (Table 5).

A comparative study was performed for the use of 20% PMo_7W_5/kaolin with some of the reported catalysts for the synthesis of 6-methyl-2-oxo-4-aryl-1,2,3,4-tetrahydropyrimidine-5-carboxylate (Table 6). Reaction with different catalysts required a higher amount of catalyst and longer reaction times compared with 20% PMo_7W_5/kaolin in solvent-free systems. In most methods, the reaction was achieved in solvent such as ethanol, acetic acid and dioxane. Thus, 20% PMo_7W_5/kaolin encouraged the reactions more effectively than the other catalysts and should be considered as one of the top choices for selecting an economically convenient, user-friendly catalyst.

3.3 Recycling of the catalyst

One of the most important features of the present methodology is the recyclability of the catalyst. It was observed that the 20%

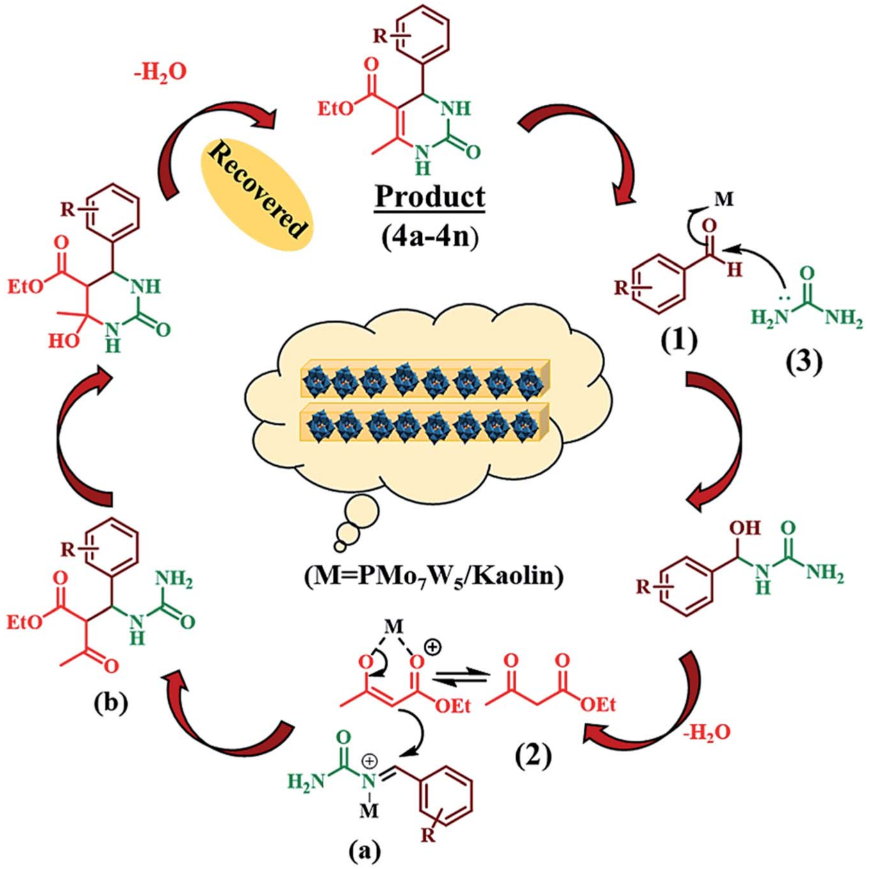

Scheme 4 Proposed mechanism for the synthesis of 3,4-dihydropyrimidin-2(1*H*)-ones.

PMo_7W_5/kaolin catalyst could be reused multiple times. For this purpose, the same model reaction was performed again studied under the optimized conditions (Table 7). After reaction completion, the reaction mixture was diluted using hot ethanol and filtered for catalyst separation, the solid catalyst was washed with ethanol several times, dried and calcined at 200 °C for 5 h and reused for subsequent reaction. The results (Fig. 8) revealed that the catalyst exhibited good catalytic activity up to six consecutive cycles.

The FT-IR and XRD spectra of the recovered 20% PMo_7W_5/kaolin (after six cycles) were matched with those of the fresh sample. As documented in Fig. 7, the FT-IR showed two bands at 938 and 910 cm^{-1} were found to similar of fresh 20% PMo_7W_5/kaolin (Fig. 7a *verses* Fig. 1). XRD spectra displayed by the recovered 20% PMo_7W_5/kaolin catalyst at $2\theta = 20.12°$, 21.97°, 23.65, 25.63°, 35.53° and 59.32° were found to be almost similar to the fresh one (Fig. 7b *verses* Fig. 2).

3.4 Plausible reaction mechanism

The possible reaction pathway for the Biginelli three-component condensation mediated by 20%PMo_7W_5/kaolin was depicted in Scheme 4. The first step involves nucleophilic attack of urea (3) on the electron deficient carbon of aldehyde (1). Here, electrophilicity of carbonyl group of aldehyde increased due to Brönsted and Lewis acidic nature of 20% PMo_7W_5/kaolin, which leads to formation of *N*-acyliminium ion intermediate (a). Interception of this iminium ion intermediate by activated 1,3-dicarbonyl compound (2) produces an open-chain ureide (b) which subsequently undergoes cyclization and dehydration to afford the corresponding dihydropyrimidinones.

4. Conclusion

In conclusion, we have successfully synthesis a series of tungsten-substituted molybdophosphoric acid ($H_3PMo_7W_5O_{40}\cdot 24H_2O$) catalyst impregnated with acidified kaolin clay. The catalytic activity of PMo_7W_5/kaolin was probed through one-pot synthesis of 3,4-dihydropyrimidin-2(1*H*)-ones *via* Biginelli reaction. The 20% PMo_7W_5/kaolin showed higher catalytic activity than the bulk PMo_7W_5 catalyst, as well as the 10% and 15% PMo_7W_5/kaolin. The effects of various parameters such as catalyst loading, amount of catalyst, effect of solvents, influence of temperature on the rate of reaction, comparison of different catalyst was discussed in detail. The 20% PMo_7W_5/kaolin catalyst shows very high conversion rates in short reaction times. This catalyst was recovered easily from reaction mixture and reused at least six times without significant loss of its catalytic activity. Therefore, the newly synthesised 20% PMo_7W_5/kaolin could be used as a promising heterogeneous catalyst for a wide range of multifunctional applications.

Conflicts of interest

There are no conflicts to declare.

Acknowledgements

The author DSA is gratefully acknowledges the University Grant Commission (UGC), New Delhi (India) for senior research fellowship (SRF). SGS is thankful to Dr Babasaheb Ambedkar Marathwada University, Aurangabad (MS), India (STAT/VI/RG/DEPT/2019-20/337-38) and UGC-DST SAP for financial assistance. We are also thankful to Department of Chemistry, Dr Babasaheb Ambedkar Marathwada University, Aurangabad (MS), India for providing laboratory facility.

Notes and references

1 H. R. Gurav, K. Y. Nandiwale and V. V. Bokade, *J. Phys. Org. Chem.*, 2014, **27**, 121–127.
2 R. Chen, J. Xin, D. Yan, H. Dong, X. Lu and S. Zhang, *ChemSusChem*, 2019, **12**, 2715–2724.
3 J. L. Horan, A. Genupur, H. Ren, B. J. Sikora, M.-C. Kuo, F. Meng, S. F. Dec, G. M. Haugen, M. A. Yandrasits, S. J. Hamrock, M. H. Frey and A. M. Herring, *ChemSusChem*, 2009, **2**, 226–229.
4 J. Li, X. Wang, W. Zhu and F. Cao, *ChemSusChem*, 2009, **2**, 177–183.
5 N. L. Mulik, P. S. Niphadkar, K. V. Pandhare and V. V. Bokade, *ChemistrySelect*, 2018, **3**, 832–836.
6 R. Chaudhary and M. Datta, *J. Anal. Sci., Methods Instrum.*, 2013, **03**, 193–201.
7 M. M. Heravi, M. Mirzaei, S. Y. S. Beheshtiha, V. Zadsirjan, F. Mashayekh Ameli and M. Bazargan, *Appl. Organomet. Chem.*, 2018, **32**, 1–10.
8 E. G. Zhizhina, Y. A. Rodikova, O. Y. Podyacheva and Z. P. Pai, *Z. Anorg. Allg. Chem.*, 2018, **644**, 869–876.
9 N. C. Coronel, M. J. da Silva, S. O. Ferreira, R. C. da Silva and R. Natalino, *ChemistrySelect*, 2019, **4**, 302–310.
10 W.-S. Che, H.-H. Gai, W.-B. Hao and R.-H. Ma, *Synth. React. Inorg., Met.-Org., Synth. React. Inorg., Met.-Org., Nano-Met. Chem.*, 2014, **44**, 649–655.
11 S. Bencedira, O. Bechiri, M. Djenouhat and M. Boulkra, *Arabian J. Sci. Eng.*, 2020, **45**, 4669–4681.
12 S. Tang, W. Wu, Z. Fu, S. Zou, Y. Liu, H. Zhao, S. R. Kirk and D. Yin, *ChemCatChem*, 2015, **7**, 2637–2645.
13 C. L. Hill and C. M. Prosser-McCartha, *Coord. Chem. Rev.*, 1995, **143**, 407–455.
14 J. Xu, R. W. Gable and C. Ritchie, *Acta Crystallogr.*, 2018, **74**, 1384–1389.
15 M. Chamack, A. R. Mahjoub and H. Aghayan, *Chem. Eng. J.*, 2014, **255**, 686–694.
16 H. Fakhri, A. R. Mahjoub and H. Aghayan, *J. Radioanal. Nucl. Chem.*, 2019, **321**, 449–461.
17 H. Aghayan, A. R. Khanchi, T. Yousefi and H. Ghasemi, *J. Nucl. Mater.*, 2017, **496**, 207–214.
18 H. Wu, M. Zhou, Y. Qu, H. Li and H. Yin, *Chin. J. Chem. Eng.*, 2009, **17**, 200–206.
19 I. V. Kozhevnikov, *Chem. Rev.*, 1998, **98**, 171–198.
20 A. D. Newman, D. R. Brown, P. Siril, A. F. Lee and K. Wilson, *Phys. Chem. Chem. Phys.*, 2006, **8**, 2893.

21 L. H. O. Pires, A. N. de Oliveira, N. Alex Jr, R. S. Angelica, C. E. F. da Costa, J. R. Zamian, L. A. S. do Nascimento and G. N. R. Filho, *Appl. Catal., B*, 2014, **160–161**, 122–128.

22 T. Suppan, M. K. Kunjunni, A. Barik and R. R. Bhattacharjee, *ChemistrySelect*, 2018, **3**, 1275–1281.

23 L. Muraleedharan, Bellundagere, M. Chandrashekara, Bangalore, S. J. Prakash, Yajnavalkya and S. Bhat, *ChemistrySelect*, 2018, **3**, 801–808.

24 A. E. R. S. Khder, H. M. A. Hassan and M. S. El-Shall, *Appl. Catal., A*, 2012, **411–412**, 77–86.

25 D. S. Park, B. K. Kwak, N. D. Kim, J. R. Park, J. H. Cho, S. Oh and J. Yi, *ChemCatChem*, 2012, **4**, 836–843.

26 A. G. Olaremu, *J. Miner. Mater. Charact. Eng.*, 2015, **03**, 353–361.

27 S. Yahaya, S. S. Jikan, N. A. Badarulzaman and A. D. Adamu, *Path Sci.*, 2017, **3**, 1001–1004.

28 S. Attique, M. Batool, M. I. Jalees, K. Shehzad, U. Farooq, Z. Khan, F. Ashraf and A. T. Shah, *Turk. J. Chem.*, 2018, **42**, 684–693.

29 J. P. Nguetnkam, R. Kamga, F. Villiéras, G. E. Ekodeck, A. Razafitianamaharavo and J. Yvon, *J. Colloid Interface Sci.*, 2005, **289**, 104–115.

30 S. K. Kundu, J. Mondal and A. Bhaumik, *Dalton Trans.*, 2013, **42**, 10515–10524.

31 L. Chen, B. Nohair, D. Zhao and S. Kaliaguine, *ChemCatChem*, 2018, **10**, 1918–1925.

32 K. S. Atwal, B. N. Swanson, S. E. Unger, D. M. Floyd, S. Moreland, A. Hedberg and B. C. O'Reilly, *J. Med. Chem.*, 1991, **34**, 806–811.

33 J. Azizian, M. K. Mohammadi, O. Firuzi, B. Mirza and R. Miri, *Chem. Biol. Drug Des.*, 2010, **75**, 375–380.

34 A. T. Khan, M. Lal, S. Ali and M. M. Khan, *Tetrahedron Lett.*, 2011, **52**, 5327–5332.

35 C. O. Kappe, *Eur. J. Med. Chem.*, 2000, **35**, 1043–1052.

36 X. Chen and Y. Peng, *Catal. Lett.*, 2008, **122**, 310–313.

37 S. L. Jain, J. K. Joseph and B. Sain, *Catal. Lett.*, 2007, **115**, 52–55.

38 C. Ramalingan, S. J. Park, I. S. Lee and Y. W. Kwak, *Tetrahedron*, 2010, **66**, 2987–2994.

39 F. Tamaddon, Z. Razmi and A. A. Jafari, *Tetrahedron Lett.*, 2010, **51**, 1187–1189.

40 D. S. Aher, K. R. Khillare, L. D. Chavan and S. G. Shankarwar, *ChemistrySelect*, 2020, **5**, 7320–7331.

41 O. D. S. Lacerda, R. M. Cavalcanti, T. M. de Matos, R. S. Angélica, G. N. da Rocha Filho and I. D. C. L. Barros, *Fuel*, 2013, **108**, 604–611.

42 L. V. Chopda and P. N. Dave, *ChemistrySelect*, 2020, **5**, 2395–2400.

43 D. S. Aher, K. R. Khillare, L. D. Chavan and S. G. Shankarwar, *ChemistrySelect*, 2020, **5**, 7320–7331.

44 L. Rozic, B. Grbic, S. Petrovic, N. Radic, L. Damjanovic and Z. Vukovic, *Mater. Chem. Phys.*, 2015, **167**, 42–48.

45 A. B. Gawade, M. S. Tiwari and G. D. Yadav, *ACS Sustainable Chem. Eng.*, 2016, **4**, 4113–4123.

46 V. V. Bokade and G. D. Yadav, *Appl. Clay Sci.*, 2011, **53**, 263–271.

47 G. Yadav, *J. Catal.*, 2003, **217**, 88–99.

48 Z. Xie, H. Wu, Q. Wu and L. Ai, *RSC Adv.*, 2018, **8**, 13984–13988.

49 H. Cai, X. Wu, Q. Wu and W. Yan, *Dalton Trans.*, 2016, **45**, 14238–14242.

50 D. L. Da Silva, S. A. Fernandes, A. A. Sabino and A. De Fa, *Tetrahedron Lett.*, 2011, **52**, 6328–6330.

51 R. Tayebee and M. Ghadamgahi, *Arabian J. Chem.*, 2017, **10**, S757–S764.

52 H. Khabazzadeh, E. T. Kermani and T. Jazinizadeh, *Arabian J. Chem.*, 2012, **5**, 485–488.

53 M. M. Heravi, F. Derikvand and F. F. Bamoharram, *J. Mol. Catal. A: Chem.*, 2005, **242**, 173–175.

54 Y. Zhang, B. Wang, X. Zhang, J. Huang and C. Liu, *Molecules*, 2015, **20**, 3811–3820.

55 F. Zamani and E. Izadi, *Catal. Commun.*, 2013, **42**, 104–108.

56 J. Safaei Ghomi, R. Teymuri and A. Ziarati, *Monatsh. Chem.*, 2013, **144**, 1865–1870.

57 R. J. Kalbasi, A. R. Massah and B. Daneshvarnejad, *Appl. Clay Sci.*, 2012, **55**, 1–9.

58 J. Mondal, T. Sen and A. Bhaumik, *Dalton Trans.*, 2012, **41**, 6173.

59 Z.-J. Quan, Y.-X. Da, Z. Zhang and X.-C. Wang, *Catal. Commun.*, 2009, **10**, 1146–1148.